

Tensor network study of deconfined quantum criticality in a one-dimensional spin-phonon model

Anton Romen,^{1,2} Josef Willsher,³ David Hofmeier,⁴ Johannes Knolle,^{1,2} and Michael Knap^{1,2}

¹*Technical University of Munich, TUM School of Natural Sciences, Physics Department, 85748 Garching, Germany*

²*Munich Center for Quantum Science and Technology (MCQST), Schellingstr. 4, 80799 München, Germany*

³*Max-Planck-Institut für Physik komplexer Systeme, Nöthnitzer Straße 38, 01187 Dresden, Germany*

⁴*Center for Quantum Mathematics, University of Southern Denmark, Campusvej 55, 5230 Odense, Denmark*

(Dated: June 8, 2026)

Deconfined quantum critical points (DQCPs) describe continuous transitions between ordered phases beyond the Landau paradigm. A simple example is the Néel antiferromagnet (AFM) to valence bond solid (VBS) transition in a 1D antiferromagnetic $J_1 - J_2$ model. In analogy to the spin-Peierls instability of critical spin chains, DQCPs are predicted to be unstable towards lattice distortions below a critical phonon frequency. In this work, we use tensor network simulations to investigate this instability in the antiferromagnetic $J_1 - J_2$ model coupled to lattice vibrations. We confirm the stability of DQCP for large phonon frequencies and demonstrate that the transition turns strongly first-order below a critical frequency. The instability is caused by a reduction of the Luttinger parameter due to spin-phonon interactions and we identify the effective theory of the behavior as the double sine-Gordon model. The same effective theory is known to describe the classical Ashkin-Teller model, which enables us to show that the critical endpoint is in the four-state Potts universality class. Furthermore, we provide quantitative numerical scaling results for the phonon spectral function, offering an experimental signature to probe DQCP-phonon coupling in low-dimensional materials.

I. INTRODUCTION

Deconfined quantum criticality (DQC) was originally introduced [1, 2] as a non fine-tuned continuous transition between an antiferromagnetic Néel state (AFM) and a dimerized valence bond solid (VBS) in a frustrated magnet on the square lattice. This should be contrasted with Landau-Ginzburg theory in which such direct transitions between phases that break different symmetries are fine-tuned [3, 4]. More generally, DQC has been proposed as a powerful tool to organize competing phases and their transitions in various contexts [5–15]. The scenario of DQC emerges from topological defects of one ordered phase that carry the charge of the other phase [16, 17]. These excitations admit a description in terms of fractionalized spinons coupled to emergent gauge fields, which become deconfined at the critical point. Additionally, emergent continuous symmetries at the transition are believed to be a defining feature of these exotic phase transitions [18, 19].

In analogy to the 2D case, recent work [20, 21] has proposed a 1D analogue of DQC, which allows an interpretation in terms of an unstable Luttinger liquid [22] that flows to different ordered phases upon tuning the sign of a single relevant perturbation. A paradigmatic example of such a transition is the AFM-VBS transition in the $J_1 - J_2$ spin chain with strong easy-axis anisotropy [23, 24]. In this setting, the low-energy effective theory takes the form of a sine-Gordon model [22]. Varying the microscopic parameters induces a sign change in the relevant perturbation and selects the type of the ordered phase. The transition occurs precisely at the sign change, where the perturbation vanishes and the remaining action is that of a Luttinger liquid with an emergent $U(1)$

symmetry. The same long-wavelength theory also arises in other microscopic realizations of 1D DQC [25].

It is well known that a spin-1/2-chain realizing a gapless phase, i.e., the Luttinger liquid, is unstable against distortions of the underlying lattice [22, 26–28], by a mechanism called the spin-Peierls instability [26, 29]. The same mechanism has also recently been discussed in the context of critical 2D spin liquids [30, 31]. A simple energetic argument shows that the chain can lower its energy by dimerization forming singlet states, thereby realizing the gapped VBS phase. The same reasoning can also be extended to a gapless phase transition, like the aforementioned DQCP. Therefore, one may reasonably suspect that the 1D DQCP is generically unstable with the transition turning first-order when taking into account lattice degrees of freedom. Indeed, in a recent work [32] it was argued, based on a low-energy field theoretical framework, that an analog of the spin-Peierls instability is also expected for DQC in the case of coupling to phonons: Static distortions of the underlying lattice geometry turn the transition strongly first order. This instability is potentially lifted upon adding dynamics of the underlying lattice; considering dynamical phonon excitations of the lattice, it has been argued that DQC remains stable above a critical phonon frequency [32].

In this context, recent numerical studies on 2D systems indeed suggest that DQC and critical quantum spin liquids show confining behavior as a function of phonon frequency [31, 33]. This highlights that further work is needed to understand the fate of deconfined phase transitions and emergent symmetries under the presence of phonon coupling. In this work, we aim to understand the mechanisms of such a deconfined phase transition turning strongly first order when coupled to lattice degrees of

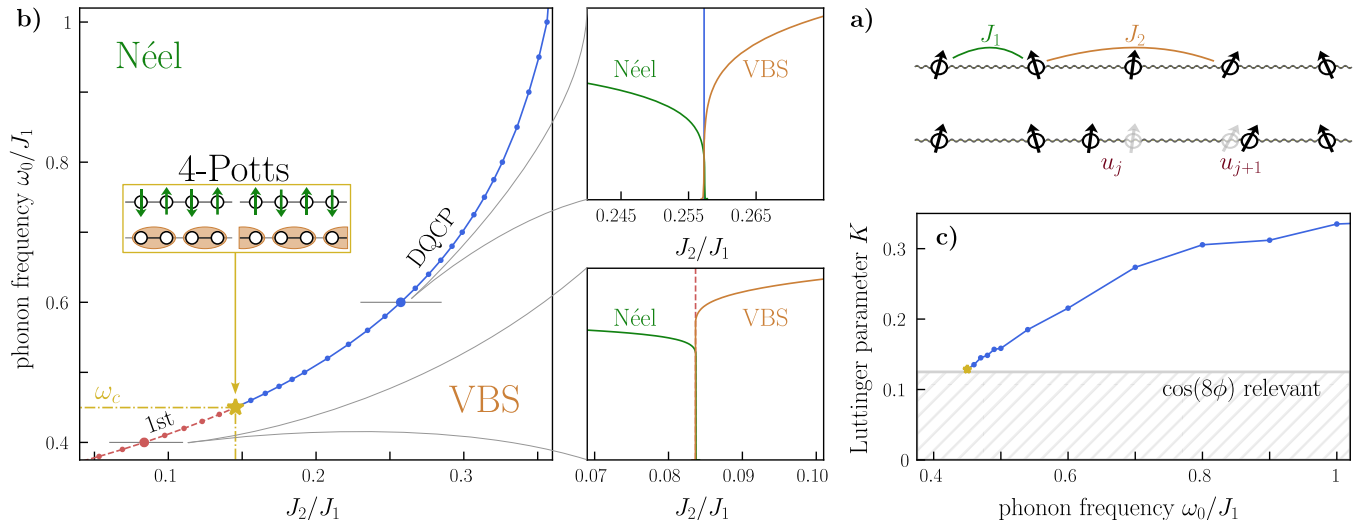


FIG. 1. Phase Diagram of a frustrated 1D spin-chain coupled to quantum phonons: a) We consider a 1D spin chain with antiferromagnetic nearest and next-nearest neighbor interactions and strong spin anisotropy $\Delta = 4$. Spins are coupled to lattice distortions, modeled by site phonons with displacement u_j at a single variable frequency ω_0 . b) Above the critical frequency ω_c , the spin-phonon model realizes a line of deconfined quantum critical points with varying critical exponents between an Ising-Néel ordered phase and a dimerized valence bond solid. The critical line ends at ω_c , marked by an endpoint in the four-state Potts universality class. Below ω_c the transition turns strongly first-order. Typical cuts at fixed ω_0 show differing behavior of the order parameters. At the first order transition, the order parameters jumps discontinuously at the transition. Conversely, along the line of DQCPs, the order parameters continuously vanish at the critical point. c) The dominant effect of dynamical phonons is a reduction of the Luttinger parameter K as function of frequency. The endpoint of the critical line is marked by a Luttinger parameter $K = 1/8$, where the next symmetry-allowed term $\cos(8\phi)$ becomes relevant in the continuum action.

freedom by focusing on a one-dimensional model, allowing us to perform both analytic and numerical analyses. With this complementary insight we are able to understand the nature of the DQC-endpoint and predict the consequences of the low-frequency confining phase.

A. Summary of main results

We study a prototypical 1D spin-chain coupled to phonons and determine the full phase diagram of this model shown in Fig. 1 using tensor network simulations by implementing the phonons as truncated bosonic sites. Our numerics is consistent with the DQCP persisting above a critical phonon frequency ω_c . We further extract the dynamically varying Luttinger parameter K which enables us to relate the breakdown of DQC to a reduction of the Luttinger parameter resulting from spin-phonon coupling.

We argue that the critical endpoint of the continuous DQCP lies in the four-state Potts universality class and is described by the same effective double-frequency sine-Gordon theory as the high-symmetry critical point of the Ashkin-Teller model [34–36]. Contrary to the Ashkin-Teller model that develops an intermediate phase beyond the endpoint, our model realizes a strong first-order transition. Based on a classical analysis of the double-frequency sine-Gordon model, we show that the nature of the transition depends on the prefactor ρ of the double

frequency $-\rho \cos(8\phi)$ term: In the Ashkin-Teller model, the sign of ρ is fixed to be *negative*, which causes the line of continuous transitions to split into two Ising transitions. By contrast, a *positive* prefactor introduces a potential barrier at the critical point when the $\cos(8\phi)$ term is relevant, turning the DQCP strongly first order.

Our work further provides insight into the physical effects of spin-phonon coupling by computing the phonon spectral function across the continuous and first-order transition. We study how spin fluctuations modify the spectral properties of the phonons. A famous example of this is the Kohn anomaly of low-dimensional electron systems which is a discontinuity of the phonon dispersion due to (critical) fluctuations in a coupled electron system [37]. The Kohn anomalies in the free electron chain and in (interacting) spin chains provide another perspective on the (spin-)Peierls instability: Increasing the spin/electron-phonon coupling acts to renormalize the phonon self energy, until it eventually condenses when the gap closes. In our numerics, we indeed observe a Kohn anomaly in the phonon dispersion across the DQCP. This manifests as a kink in the phonon spectrum in the ordered phases, as well as the emergence of a critical continuum at low frequencies at the deconfined transition. We measure the phonon spectral function $A(q, \omega)$ and find that at the critical point, spin-phonon coupling leads to a hybridization with the dimer-fluctuations [38], such that a universal power-law response emerges $A(q = \pi, \omega) \sim \omega^{-2K}$, governed by the Luttinger parameter of the transition.

B. Structure of the work

The work is organized as follows: In Sec. II we introduce the spin-phonon model and discuss various limiting cases. First, we analyze the static limit of the decoupled spin chain in Sec. II A that realizes a DQCP between an AFM and VBS phase and give a brief summary on DQCP in (1+1)D. We then establish in Sec. II B how spin-phonon coupling naturally emerges in this model and introduce suitable approximations for the phonon and spin-phonon Hamiltonians. In Sec. II C we consider the adiabatic limit of the coupled spin-phonon model, akin to static lattice distortions. In this limit, lattice vibrations can be treated classically, resulting in a static spin Hamiltonian with dimerized nearest-neighbor interactions and a quadratic potential energy cost. We use this model to give a brief overview of the well known Peierls instability and recapitulate predictions from Ref. [32] that the DQCP turns strongly first-order on a distorted lattice. We provide numerical data supporting this scenario. In Sec. III we extend the analysis to the general case of dynamical spin-phonon coupling. We determine the phase diagram of the model and link the nature of the transition to the flow of the Luttinger parameter as summarized in Fig. 1. We provide an analysis of the critical endpoint of the DQC line and link the low-energy theory of the model to the static limit. In Sec. IV, we analyze the phonon spectral function, and find numerical evidence for the emergence of a critical continuum in the second-order regime and large weight at small frequencies in the other regime, consistent with a 1st order transition. This also provides a powerful observable to investigate spin-phonon coupling in scattering experiments. We provide a summary of results and outlook for future work in Sec. V. Technical details are relegated to the appendices.

II. SPIN-PHONON MODEL: LIMITING CASES

We consider a one-dimensional, coupled spin-lattice system

$$H = H_s + H_p + H_{sp}, \quad (1)$$

where H_s describes the spin Hamiltonian, H_p the phonon Hamiltonian of lattice vibrations, and H_{sp} the associated spin-phonon coupling. We will introduce the exact forms below in Eqs. (2), (7) and (9).

We introduce the model in steps by looking into various limiting cases. First, we discuss the decoupled spin model H_s , corresponding to the limit of a *regular lattice* in a phonon-free model and demonstrate that it realizes a DQCP between a Néel antiferromagnet and valence bond solid, similar to Ref. [23]. In this context, we will also introduce the numerical method used to study the spin-phonon model and the lattice and continuum theories of DQCP in 1D. We then proceed with a general discussion on spin-lattice coupling and introduce models for H_p and

H_{sp} . After that, we investigate the adiabatic limit, corresponding to lattice vibrations of infinitesimal energy cost. The result is a staggered spin Hamiltonian of *static* lattice distortions, which we use to illustrate an analog of the spin-Peierls instability for DQCP. The fully dynamical spin-phonon model will be investigated in the next section.

A. Phonon-free limit: Deconfined quantum criticality

1. Spin Hamiltonian

The spin-part of our model is defined by the following spin-1/2 chain

$$H_s = J_1 \sum_j [\mathbf{S}_j \cdot \mathbf{S}_{j+1} + (\Delta_1 - 1) S_j^z S_{j+1}^z] + J_2 \sum_j [\mathbf{S}_j \cdot \mathbf{S}_{j+2} + (\Delta_2 - 1) S_j^z S_{j+2}^z] \quad (2)$$

with nearest neighbor J_1 and next-nearest neighbor J_2 exchange couplings. The parameters $\Delta_{1,2}$ are XXZ anisotropy parameters, which we take to be equal $\Delta \equiv \Delta_1 = \Delta_2$ unless specified otherwise. The regime of interest for this work will be $\Delta > 1$, where it is well known that the $J_2 = 0$ limit realizes an antiferromagnet with Néel order (AFM). Increasing J_2/J_1 introduces frustration into the AFM ground state and drives the model towards a valence-bond-solid (VBS) ground state, consisting of singlets on every second bond.

2. Continuum field theory

We can describe the long-wavelength behavior of the model introduced in Eq. (2) as a sine-Gordon model by using a standard Jordan-Wigner transformation and bosonization [22], as briefly outlined in Appendix A. It produces a low-energy description in terms of a compact bosonic field $\phi(x) \in [0, 2\pi]$, with the action

$$S_{\text{SG}} = \int dx d\tau \left[\frac{1}{2\pi K} ((\partial_x \phi)^2 + (\partial_\tau \phi)^2) - \mu \cos(4\phi) \right]. \quad (3)$$

The parameter K is the Luttinger parameter, whose precise value is determined by the microscopic couplings J_1, J_2 and Δ . The scaling dimension of the coupling μ is determined by the Luttinger parameter and given by $[\mu] = 4K$; therefore, the interaction $\cos(4\phi)$ is *irrelevant* ($[\mu] > 2$) when $K > 1/2$. The value of the coupling $\mu \sim 2J_1\Delta - 2J_2(2 + \Delta)$ is likewise determined by the parameters of the microscopic theory; for the nearest-neighbor only model ($J_2 = 0$) the interaction is irrelevant for $\Delta \leq 1$. This theory flows to a conformal fixed point with an emergent U(1) symmetry, called the Luttinger liquid phase of the XXZ chain [22]. In this regime, the

sine-Gordon model in Eq. (3) flows in the infra-red (long-distance limit) to the compact boson CFT with central charge $c = 1$ and compactification radius determined by the Luttinger parameter K .

If instead we consider theories with XXZ anisotropy $\Delta > 1$, we find that the interaction $\cos(4\phi)$ is now *relevant*. The result is a gapped phase, with order determined by the sign of μ . The competing order parameters of the spin model in Eq. (2) can be written directly in terms of the bosonic continuum field $\phi(x_j)$. We are interested in the Néel (M_j^z) and valence-bond (Ψ_j) order parameters, defined as

$$\begin{aligned} M_j^z &\equiv (-1)^j S_j^z \sim \cos(2\phi(x_j)), \\ \Psi_j &\equiv \mathbf{S}_j \mathbf{S}_{j+1} - \mathbf{S}_{j+1} \mathbf{S}_{j+2} \sim \sin(2\phi(x_j)). \end{aligned} \quad (4)$$

Using these mappings, we may rewrite the interaction in Eq. (3) as

$$-\mu \cos(4\phi) = \mu [\sin^2(2\phi) - \cos^2(2\phi)] = \mu(\Psi^2 - M_z^2), \quad (5)$$

such that Néel order is preferred when $\mu > 0$, and dimer order when $\mu < 0$. For the nearest-neighbor model ($J_2 = 0$), bosonization predicts $\mu > 0$ and we recover the gapped Ising-Néel ground state. Increasing J_2/J_1 introduces frustration and drives the model towards a dimerized phase. By tuning appropriate parameters in the microscopic Hamiltonian, it is possible to cause a sign change in μ and drive a transition to valence bond order. The critical point $\mu = 0$ is described by the same sine-Gordon continuum action as the Luttinger liquid, but with a Luttinger parameter $K < 1/2$. The gap opens with exponent $|\mu|^{\nu_\mu}$, where $\nu_\mu^{-1} = 2 - 4K$. The order parameters onset with power-law behavior $M^z, \Psi \sim |\mu|^\beta$ governed by the exponent $\beta = \nu_\mu K$. Correlations of the order parameters at the transition can be obtained from Eq. (4) using standard bosonization techniques [22]:

$$\langle M^z(0)M^z(r) \rangle \sim \langle e^{2i\phi(0)\phi(r)} \rangle \sim r^{-2K} \quad (6)$$

and similarly $\langle \Psi(0)\Psi(r) \rangle \sim r^{-2K}$.

Next, we briefly comment on the symmetries of the Hamiltonian in Eq. (2). The model is invariant under lattice translations \mathbf{T}_x and possesses a $\mathbb{Z}_2 \times U(1)$ spin symmetry, corresponding to a global spin flip along the z -axis and continuous rotations in the xy -plane. Under these symmetries, the field ϕ transforms as

$$\begin{aligned} \phi &\xrightarrow{\mathbb{Z}_2} -\phi + \pi/2, \\ \phi &\xrightarrow{U(1)} \phi, \\ \phi &\xrightarrow{\mathbf{T}_x} \phi + \pi/2. \end{aligned}$$

For Luttinger parameter $K > 1/8$, the only symmetry-allowed relevant perturbation is of the form $\cos(4\phi)$. Consequently, the sine-Gordon action in (3) constitutes the most general low-energy effective theory consistent with the symmetries of the model.

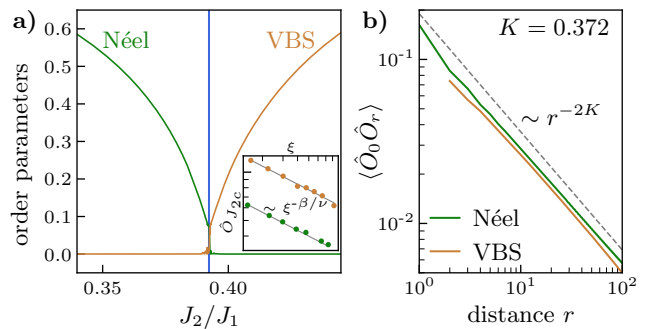


FIG. 2. **Summary of Deconfined Criticality in a 1D spin chain:** a) Upon tuning J_2/J_1 , the model undergoes a continuous transition from a gapped phase with Néel order to a dimerized VBS phase. Numerical data displays a weakly first-order transition with length scale set by the MPS correlation length ξ . Upon increasing the bond dimension χ , order parameter residuals at the transition vanish as $\hat{O}_{J_{2c}} \sim \xi(\chi)^{-\beta/\nu} \sim \xi^{-K}$ (inset), indicating a continuous transition in the thermodynamic limit, see main text for details. b) Order parameter correlations at the transitions decay algebraically, with exponent set by the Luttinger parameter K of the critical theory.

3. Numerical method

Throughout this work we simulate the model introduced in Eq. (1) using infinite-system Density Matrix Renormalization Group (iDMRG) simulations [39, 40] implemented within the TeNPy library [41] and optimize over infinite Matrix Product States (iMPS) in the thermodynamic limit [42, 43]. We provide further details on the numerical implementation in Appendix B.

Let us start by considering the spin Hamiltonian H_s in Eq. (2) at fixed $\Delta = 4$ while varying J_2/J_1 . As outlined before, we expect the ground state to have AFM order for small J_2/J_1 and VBS order at large J_2/J_1 , which can be captured by the order parameters introduced in Eq. (4). We show in Fig. 2 that the Néel order is suppressed upon increasing J_2/J_1 until the critical point $J_{2,c}/J_1 = 0.3923$, where valence bond order onsets with the same exponent. We additionally measure the critical correlations of both Néel and valence bond order parameters introduced in Eq. (6) at the transition and find good agreement with a power-law described by a Luttinger parameter $K = 0.372$.

Following arguments introduced in Ref. [21], we confirm that this transition is second order in the thermodynamic limit. For an iMPS, any finite bond dimension χ introduces an effective length scale $L_{\text{eff}} \sim \xi(\chi)$ set by the correlation length of the variational ground state. Consequently, the resulting transition can never be truly continuous at finite χ and the order parameters acquire a finite residual $\hat{O}_{J_{2c}}$ at the critical point. As we expect a second-order transition, the residuals should vanish as a function of systems size L as $\hat{O}_{J_{2c}} \sim L^{-\beta/\nu_\mu} \sim \xi(\chi)^{-\beta/\nu_\mu} \sim \xi(\chi)^{-K}$ with bond dimension χ .

In practice, the correlation length of an MPS in the thermodynamic limit is obtained from the transfer matrix [41, 44]. Additionally, the residuals are controlled using a sweep protocol in which the transition is approached from within one of the ordered phases. In each simulation, the previous ground state is used as initial state for the subsequent run. In proximity to the critical point, this procedure induces hysteresis and fixes the type of residual. The method, in fact, provides a surprisingly robust way to compute the relevant Luttinger parameter K [21, 25], see Fig. 2. We explicitly confirm that estimates for K obtained from the order parameter residuals and critical order parameter correlations agree; c.f., inset of Fig. 2 a).

B. Spin-phonon coupling

We now introduce models for H_p and H_{sp} in Eq. (1) to capture the effect of spin-phonon coupling on the DQCP.

1. Phonons

We start by introducing the distortions of lattice sites around their equilibrium positions $u_j = x_j - \bar{x}_j$, which we assume to be small. Within the harmonic approximation, u_j may then be modeled by dissipationless, uncoupled Einstein phonons at some frequency ω_0 via a phonon Hamiltonian

$$H_p = \sum_j \frac{p_j^2}{2m} + \frac{1}{2} m \omega_0^2 u_j^2. \quad (7)$$

By introducing appropriate raising and lowering operators $u_j = 1/\sqrt{(2m\omega_0)}(a + a^\dagger)$, H_p in second quantized form is given by

$$H_p = \omega_0 \sum_j a_j^\dagger a_j + \text{const.} \quad (8)$$

We will use this form to simulate the lattice degrees of freedom as boson-sites truncated at some maximal occupation. We note that instabilities of the DQCP occur at wavevector $q = \pi$, which *a posteriori* justifies considering a single (finite) phonon frequency ω_0 as a good approximation for the (generally flat and gapped) phonon band around the edge of the Brillouin zone $q \approx \pi$. In a next step, we will study how vibrations of the underlying lattice affect the exchange constants J_1 and J_2 .

2. Spin-phonon coupling

We first note that the origin of Heisenberg-type spin-spin interactions is through exchange interactions of neighboring spinful orbitals. The corresponding exchange constants are naturally bond-length dependent

and we may for example model $J_{i,j} \sim J_0 e^{-\tilde{g}|x_i - x_j|}$ in terms of the atomic positions x_j . This spatial dependence is used implicitly in Eq. (2) in the sense that $J_1 = J_0 e^{-a}$, $J_2 = J_0 e^{-2a}$, with some lattice constant $a = \bar{x}_{i+1} - \bar{x}_i$, where we assumed a regular lattice with equilibrium positions \bar{x}_j .

Finite displacements ($u_j \ll a$) of the lattice sites render the exchange constants site dependent. To linear order, the nearest neighbor exchange constant J_1 acquires a correction

$$J_1 \rightarrow J_{j,j+1} = J_0 e^{-\tilde{g}|x_j - x_{j+1}|} = J_0 e^{-\tilde{g}(a + u_{j+1} - u_j)} \\ \approx J_1 [1 + \tilde{g}(u_j - u_{j+1})].$$

This motivates the following form for the Heisenberg spin-phonon coupling:

$$H_{sp} = J_1 \tilde{g} \sum_j (u_j - u_{j+1}) [\mathbf{S}_j \cdot \mathbf{S}_{j+1} + (\Delta - 1) S_j^z S_{j+1}^z] \\ = \frac{g}{\sqrt{\omega_0}} \sum_j (a_j + a_j^\dagger - a_{j+1} - a_{j+1}^\dagger) \times \quad (9) \\ [\mathbf{S}_j \cdot \mathbf{S}_{j+1} + (\Delta - 1) S_j^z S_{j+1}^z],$$

where we have introduced $g = J_1 \tilde{g} / \sqrt{2m}$. Here, we neglected modifications of J_2 , which is justified by the observation that lattice configurations are staggered $u_j = (-1)^j u$, such that the bond length of next-nearest neighbors remains.

C. Adiabatic limit: Spin-Peierls instability

We start to build some intuition on the influence of lattice vibrations on 1D DQC by considering the adiabatic limit $\omega_0 \rightarrow 0$ in Eqs. (7) and (9), corresponding to a lattice with infinitesimal elastic energy cost.

We start with the phonon Hamiltonian in Eq. (8). For $\omega_0 \rightarrow 0$, the average number of phonons $n_p \equiv \langle a_j^\dagger a_j \rangle$ is large for any finite energy density. We can thus take the large- N limit and replace the number operator by its expectation value

$$H_p \rightarrow H_\kappa = \kappa N \delta^2 \quad (10)$$

to arrive at a harmonic potential describing the energy cost of lattice distortions. Here, we introduce an effective lattice stiffness $\kappa = m\omega_0^2$, N denotes the number of lattice sites, and $\delta \sim n_p$ measures the distortion.

Some care has to be taken for the spin-phonon coupling in Eq. (9). A state with fixed n_p has $\langle a + a^\dagger \rangle = \langle u_j \rangle = 0$. Instead, we consider coherent states $|\alpha\rangle$ to account for fluctuations around n_p , which are known to be a good approximation when taking the classical limit [45]. We thus approximate (assuming $\alpha \in \mathbb{R}$)

$$\delta_j \equiv \langle u_j \rangle = 1/\sqrt{2m\omega_0} \langle \alpha | (a_j + a_j^\dagger) | \alpha \rangle \sim \alpha / \sqrt{m\omega_0} \\ \langle \alpha | a_j^\dagger a_j | \alpha \rangle = \alpha^2 \sim m\omega_0 \delta_j^2.$$

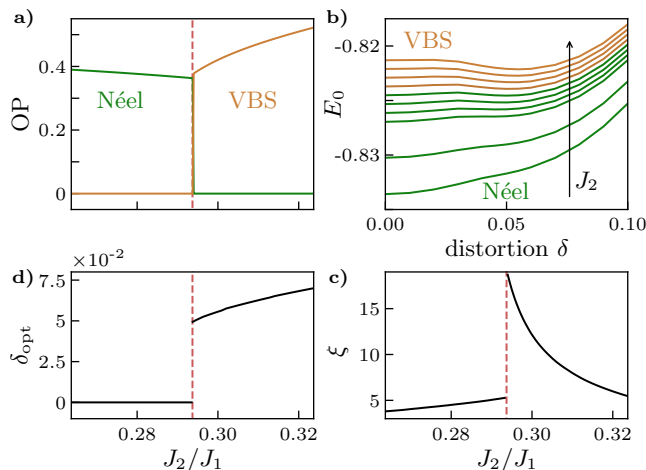


FIG. 3. **Spin-Peierls Instability of DQC in a 1D spin chain:** a) Static lattice distortions drive the DQCP to a strong first-order transition, displayed by a clear jump in the order parameter. b) Inside the VBS phase, the system favours a sudden distortion of the underlying lattice $\delta \neq 0$ to lower the ground state energy. c) The lattice instability is captured by a sudden jump of the optimal lattice distortion δ_{opt} at the transition. d) The correlation length displays clear first-order character.

Eq. (10) is recovered from the second line of the above equation by inserting the result into Eq. (8) and summing over lattice sites.

Lattice distortions can couple to the VBS order parameter with a 2-site unit cell, which motivates considering a staggered lattice distortion $\delta_j = (-1)^j \delta$. This maps $H_{sp} \rightarrow H_{\text{dim}}$ onto a dimerized spin Hamiltonian

$$H_{\text{dim}} = J_1 \sum_j \delta (-1)^j [\mathbf{S}_j \cdot \mathbf{S}_{j+1} + (\Delta - 1) S_j^z S_{j+1}^z]. \quad (11)$$

To summarize, in the adiabatic limit, the full spin-phonon Hamiltonian in Eq. (1) is mapped to a static spin Hamiltonian given by

$$H_{\text{static}}(\delta) = H_s + H_{\text{dim}}(\delta) + H_\kappa(\delta) \quad (12)$$

with H_s as defined in Eq. (2). This is a *static* model of lattice distortions which models the dimerization as a classical field, neglecting temporal fluctuations. Adding a finite lattice distortion lowers the symmetry of the Hamiltonian and allows for a more relevant operator to be present in the continuum theory [26, 28, 29]

$$S_{\text{static}}[h \sim \delta] = S_{\text{SG}} + h \int dx d\tau \sin(2\phi). \quad (13)$$

The scaling dimension of this new operator is $[h] = K$. This is relevant for all $K < 2$, and hence strongly relevant at both the Heisenberg point $K = 1/2$ as well as in the full DQCP regime $1/8 < K < 1/2$. Perturbative arguments suggest that this relevant operator will lead to an energy gain at the DQCP which always outcompetes

the cost of lattice distortions [32]. It implies spontaneous dimerization at the critical point. This has been interpreted as causing a first-order transition, but remains to be verified numerically.

To measure the competition between the lattice and spin degrees of freedom, we numerically compute the energy of the combined spin-lattice model. This energy, given by Eq. (12) has contributions from the ground state energy of a distorted spin chain, as well as the potential energy cost of the distortion, $\kappa \delta^2$ per site. To obtain the behavior of the order parameters, we calculate the energy landscape $H_{\text{static}}(\delta)$ as a function of the distortion parameter. For each J_2/J_1 , we find the distortion with the lowest energy, and calculate the order parameter of the spin chain at this optimal lattice distortion.

We now present our numerical results which confirm a spin-Peierls instability of the static spin-lattice model. Tuning J_2/J_1 at fixed lattice stiffness $\kappa = 3.5$, the order parameters jump at a critical value, consistent with a first order transition; see Fig. 3a. The landscape of the system's total energy $E_0(\delta)$ as a function of distortion parameter is shown in Fig. 3b. For low J_2/J_1 in the Néel phase, the lattice has the lowest energy at zero distortion. Upon increasing J_2/J_1 , the energy $E_0(\delta)$ develops a minimum at finite δ ; inside the VBS phase, a sudden distortion of the lattice to some $\delta_{\text{opt}} \neq 0$ lowers the energy of the ground state. We obtain the optimal lattice distortion δ_{opt} for each parameter J_2/J_1 via a quadratic fit of the energy around the minimum. In summary, we observe a clear jump in both order parameters, the optimal distortion δ_{opt} and a *finite* correlation length at the transition, consistent with a strong first order Néel-VBS transition.

III. SPIN-PHONON MODEL: DYNAMICAL PHONONS

We now turn to the full Hamiltonian introduced in Eq. (1). The effect of treating the lattice distortions as dynamical degrees of freedom is mostly unexplored beyond the Heisenberg point [46, 47]. Integrating out the dynamical phonon field generates a sine-Gordon action

$$S_{\text{SG}'} = \int dx d\tau \left[\frac{1}{2\pi K'} ((\partial_x \phi)^2 + (\partial_\tau \phi)^2) - \mu' \cos(4\phi) \right]. \quad (14)$$

with renormalized parameters $K'(\omega_0)$ and $\mu'(\omega_0)$, that depend on the phonon frequency ω_0 . We reproduce the calculation from Ref. [32] in Appendix C, and state the form of the new parameters as a function of ω_0 . Importantly, it was shown that the effect of decreasing ω_0 favors the dimer phase, and reduces the parameter $K'(\omega_0) < K$. Furthermore, it was hypothesized that this theory breaks down at the point $K'(\omega_c) = 1/8$, which defines a critical phonon frequency ω_c below which the DQCP picture breaks down. It is natural that the transition becomes first order below this point, as we just showed to be the case in the static phonon limit $\omega_0 \rightarrow 0$.

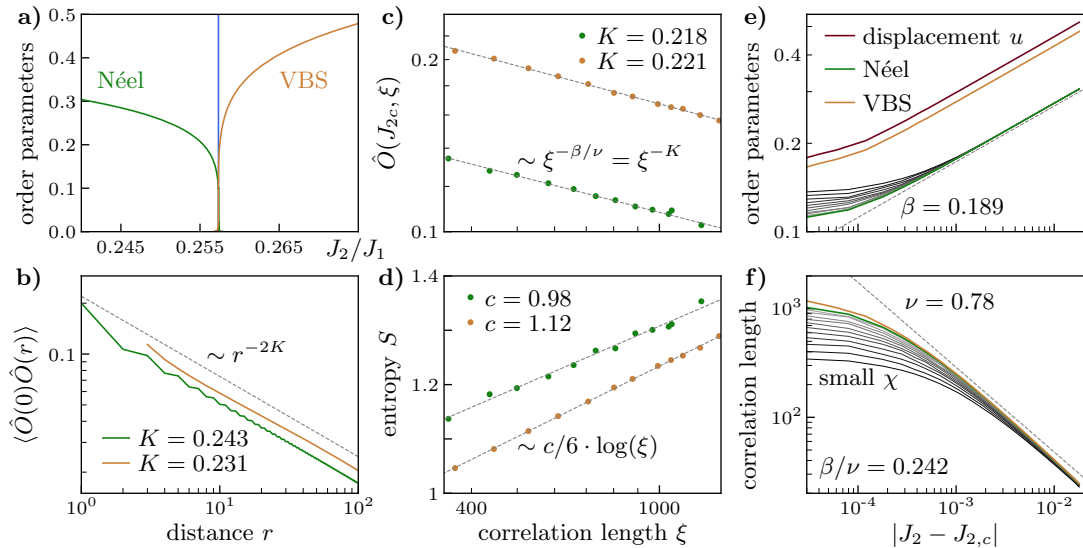


FIG. 4. **DQCP in the spin-phonon model:** a) When coupling to dynamical Einstein phonons with frequency ω_0 , the continuous transition between Néel and VBS phase persists above a critical phonon frequency ω_c . b) Order parameter correlations at the transition decay algebraically, with power law exponent $-2K$ governed by the Luttinger parameter of the critical theory. c) The order parameters develop a finite residual at the critical point, which vanishes with increasing correlation length ξ of the MPS ground state. The residuals are controlled using a sweep protocol initialized in one of the two ordered phases. Finite-size scaling predicts a power-law decay $\hat{O}_{J_{2c}} \sim \xi^{-\beta/\nu} = \xi^{-K}$, which we use to obtain an independent estimate for the Luttinger parameter. d) The entanglement entropy at the critical point scales linearly with $\log \xi$, consistent with a free Gaussian fixed point with central charge $c = 1$. e) Both spin order parameters as well as the average phonon displacement demonstrate power-law scaling in the vicinity of the transition with matching exponent β as required by the critical theory. f) Power-law behavior with increasing bond dimension χ is also observed in the correlation length and the Luttinger parameter obtained from the ratio of critical exponents is consistent with previously obtained estimates. Data obtained for $\Delta_1 = \Delta_2 = 4, g = 0.25J_1, \omega_0 = 0.6J_1$.

We now investigate the full spin-phonon model with $\Delta_1 = \Delta_2 = 4, g = 0.25J_1$. To simplify the electron-phonon coupling, we consider isotropic spin phonon interactions, $H_{sp} \rightarrow g \sum_j (a_j + a_j^\dagger - a_{j+1} - a_{j+1}^\dagger) \mathbf{S}_j \cdot \mathbf{S}_{j+1}$, *c.f.*, Eq. (9). We found this isotropic coupling to be numerically more favorable, while not changing the essential physics. We limit the maximum number of phonons per site to $N_{\max} = 6$ and confirm in Appendix D that the relevant physics does not change with increasing N_{\max} . With that, we investigate the transition by tuning J_2/J_1 for various values of ω_0/J_1 . For our iMPS, we consider bond dimensions $136 \leq \chi \leq 472$. Further details on the numerical implementation are provided in Appendix B.

A. Results of the 2nd- and 1st-order transition

In the limit $\omega_0 \rightarrow \infty$, the lattice becomes infinitely stiff, causing the spins and phonons to effectively decouple. In this limit, the spin model realizes the DQCP introduced in Fig. 2. We now show that our numerics is consistent with a continuous transition for finite $\omega_0 > \omega_c \approx 0.45J_1$.

We summarize results for the DQCP regime in Fig. 4, using a typical cut at phonon frequency $\omega_0 = 0.6J_1$. We first determine the critical point $J_{2c}(\omega_0 = 0.6J_1) \approx 0.2573J_1$, at which both order parameters continuously

vanish, see Fig. 4a. The spin-phonon coupling acts to favor the VBS phase, shifting the critical point to lower J_2/J_1 compared to the static case. The order parameter correlations at the transition show clear power-law decay; see Fig 4b. The numerically determined exponent $-2K'_c$, indicates a Luttinger parameter $K'_c \approx 0.237$, at the new critical point, where we use the subscript K'_c to emphasize that the Luttinger parameter was obtained from critical order parameter correlations. Crucially, we find a lower value of $K'_c < K = 0.372$ than in the static limit. This agrees with the prediction that spin-phonon coupling lowers the Luttinger parameter at the transition.

We further compute the order parameter residuals at the transition for various bond dimensions and confirm that the residuals agree with the finite-size scaling prediction introduced in Sec. II A, as shown in Fig 4c. We thus obtain a second estimate $K'_r(\omega_0 = 0.6J_1) \approx 0.221$ for the Luttinger parameter of the transition, consistent with the previous estimate. Additionally, we confirm the power-law behavior of the order parameters $\hat{O} \sim |J_2 - J_{2c}|^\beta$ and correlation length $\xi \sim |J_2 - J_{2c}|^{-\nu}$ close to the transition and compute the respective critical exponents β and ν , as summarized in Fig. 4e and 4f. We find that the average phonon displacement $u = 1/N \sum_j (-1)^j u_j$ follows the same power law, indicating that the lattice displacement couples linearly to the VBS order parameter. The

order parameter critical exponent β matches for both order parameters as required by the critical theory, and signals that the emergent $U(1)$ symmetry between Néel and VBS order parameter components is preserved in the presence of spin-phonon coupling, when $\omega_0 = 0.6J_1$. We find for the Luttinger parameter $K' = -\beta/\nu \approx 0.242$, in agreement with the previous estimates K'_r and K'_c obtained from the order parameter residuals and correlations at the critical point. Measurements of β and ν as a function of frequency are shown in Appendix D, Fig. 13.

Further compelling evidence for a continuous transition is found from the scaling of entanglement entropy with correlation length $\xi(\chi)$, which is expected to follow $S \sim c/6 \log(\xi)$ [48]. Numerical data shown in Fig. 4d indicate $c = 1$, in agreement with a free Gaussian fixed point of the critical theory outlined before.

Below a critical frequency $\omega_0 \leq \omega_c \approx 0.45J_1$ the transition turns strongly first-order. We show a typical 1st-order cut for $\omega_0 = 0.4J_1$ in Fig. 5. In this regime, the order parameters display a clear jump at the transition. Moreover, the MPS correlation length rapidly saturates to a finite value and the ground state energy shows a sizable discontinuity at the transition indicated by a jump in the derivative $\partial E/\partial J_2$.

To clearly distinguish the first and second order transition, we resort to an analysis of the VBS Binder cumulant [49] $U_B \equiv 1/2 \cdot (3 - \langle \Psi^4 \rangle / \langle \Psi^2 \rangle^2)$, computed for various window sizes L on the iMPS ground state. Within the ordered (disordered) phase the Binder cumulant rapidly approaches $U_B \rightarrow 1(0)$ respectively, and U_B is generally expected to be positive and scale invariant at a second-order transition. In contrast, at a first-order transition, the Binder cumulant develops a diverging negative cusp with increasing system size [49]. This divergence is a direct consequence of a multi-peak order parameter distribution arising from phase coexistence, and thus serves as an indicator for a (strong) 1st-order transition. We show the negative peak of the Binder cumulant of the VBS order parameter along the first-order cut in Fig. 5d. In our simulations, we further define the critical frequency ω_c as the lowest frequency, for which the Binder cumulant remains monotonous.

The numerical analysis of the phase diagram in the ω_0/J_1 and J_2/J_1 plane for $\Delta_1 = \Delta_2 = 4, g = 0.25J_1$ is summarized in Fig. 1, yielding the stability of the DQCP down to $\omega_0 \approx 0.45J_1$. In Appendix D, Fig. 12, we evaluate the phase diagram for an additional parameter cut $\Delta_1 = 4, \Delta_2 = 1, g = 0.15J_1$, chosen such that the Luttinger parameter is $K_s \approx 0.2$ for the DQCP of the decoupled spin model. Also for this case, we find that the continuous transition breaks down at $K' \approx 1/8$, and is hence independent of K_s .

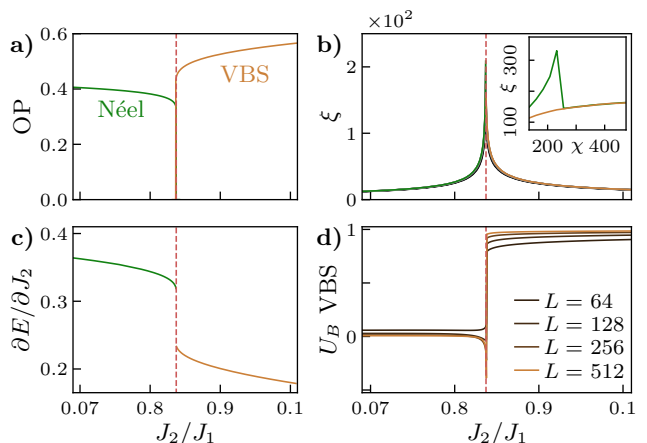


FIG. 5. **Strong first-order transition in the spin-phonon model:** Below a critical phonon frequency ω_c , the transition between Néel and VBS phase turns strongly first order. a) This is indicated by a clear jump in the order parameters, b) rapid saturation of the correlation length, and c) a discontinuity in the energy derivative at the transition. d) Further evidence for a strong-first order transition is obtained from the VBS Binder Cumulant U_B , which develops a diverging negative cusp with increasing system size. This behavior arises from a multi-peak distribution of the order parameter in the presence of phase coexistence. Data obtained for $\Delta_1 = \Delta_2 = 4, g = 0.25J_1, \omega_0 = 0.4J_1$.

B. 4-State Potts critical endpoint & first-order regime

We will now describe the universality of the critical endpoint and discuss the first-order regime in more detail. We propose that the phase diagram is described by the double sine-Gordon model, with an action given by

$$S_{\text{DSG}} = \int dx d\tau \left[\frac{1}{2\pi K} ((\partial_x \phi)^2 + (\partial_\tau \phi)^2) - \mu \cos(4\phi) - \rho \cos(8\phi) \right]. \quad (15)$$

The new interaction term (last term) has the scaling dimension $[\rho] = 16K$ and is therefore relevant when $K < 1/8$. The coupling is symmetry allowed, preserving the $\mathbb{Z}_2 \times U(1)$ spin-rotation and translation symmetry \mathbf{T}_x and will generally be generated, when taking into account higher-order terms in the boson-fermion operator expansion. In the regime $1/8 < K < 1/2$, this coupling is irrelevant and the critical line $\mu = 0$ remains gapless. This justifies neglecting this contribution in the standard bosonization approaches discussed so far. However, the presence and value of this coupling will be important for understanding the phase diagram for $\omega \leq \omega_c$. This same effective theory has been understood to describe the universal physics and phase diagram of the Ashkin-Teller model [50–53]. In that model the critical line is a $c = 1$

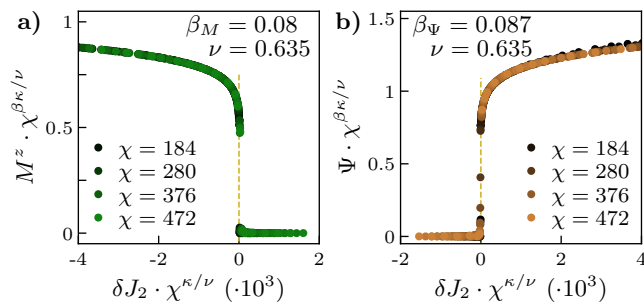


FIG. 6. **Critical exponents of the transition at the endpoint ω_c :** We employ a finite-size scaling Ansatz to obtain estimates for the order parameter exponent β and correlation length exponent ν of the transition at the critical frequency ω_c , where the DQCP line ends, both for the magnetization and VBS order parameter. From both we find $\beta \approx 0.0835$ and $\nu \approx 0.635$ in good agreement with the critical exponents of the four-state Potts universality class.

CFT, which bifurcates into two Ising CFT transitions with $c = 1/2$ at the 4-state Potts point. Bifurcation occurs at the point $K = 1/8$ (in our conventions) and is likewise a CFT with $c = 1$.

First, let us use this to understand the critical endpoint of the DQCP transition line. As shown already in Fig. 1, we measure a Luttinger parameter $K = 1/8$ at this endpoint $\omega_c = 0.45J_1$. This is compatible with the picture of the continuum field theory, which tells us that the DQCP is destroyed by the presence of a second relevant coupling ρ here. Furthermore, we can identify the dynamical exponent $\eta = 1/2$ via $K = 1/8$ at the critical endpoint. Using a finite size scaling ansatz [54]

$$\hat{O}\chi^{\beta\kappa/\nu} = F(\delta J_2\chi^{\kappa/\nu}) \quad (16)$$

for the order parameters, we obtain precise numerical estimates for $\beta_M = 0.08$, $\beta_\Psi = 0.087$ and $\nu = 0.635$, as shown in Fig. 6. The numerical values are in good agreement with the exact values $\beta = 1/12 \approx 0.083$ and $\nu = 2/3 \approx 0.667$ of the four-state Potts universality class [55–58]. Minor deviations are consistent with logarithmic corrections, which are expected to be small for the system sizes considered. We provide a justification of the finite size scaling ansatz in Appendix D and confirm the critical exponents for a sweep along the frequency direction in Fig. 14.

At low phonon frequencies, the Néel to VBS transition is strongly first order and arises from a direct level crossing of the respective ground states. At the transition point, the two Néel and two VBS states become degenerate. Notably, in this regime, the VBS ground states reside on a distorted lattice ($\langle u_j \rangle \neq 0$), even at criticality. Upon increasing the phonon frequency, the lattice distortion associated with the VBS state at the transition is suppressed. The four-state Potts endpoint is reached when the distortion approaches zero and the four degenerate ground states collapse into a single symmetric critical ground state, as summarized in Fig. 1a.

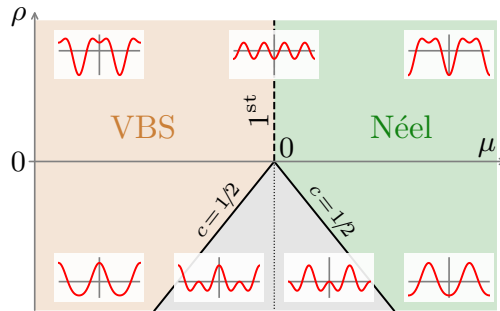


FIG. 7. **Classical phase diagram of the DSG potential:** We consider a double-frequency sine-Gordon model with relevant $-\rho \cos(8\phi)$ term. For positive values of ρ , the classical theory implies a first-order transition between the two ordered phases, identified with the VBS and AFM phase in our setting. Instead, for $\rho < 0$, an intermediate region around the original transition $\mu = 0$ is found, where the minima of the potential lie in $(0, \pi/4)$, suggesting the existence of an intermediate phase. This phase is bounded by two Ising transitions.

To obtain further insight into the structure of the phase transition, let us now analyze the effective theory Eq. (15) at a classical level [59]. The potential term in the double sine-Gordon model

$$V(\phi) = -\mu \cos(4\phi) - \rho \cos(8\phi) \quad (17)$$

has the following minima

$$\begin{cases} \phi_0 = 0, \pi/2 & \mu > 0, \rho > -\mu/4 \\ \phi_0 = \pi/4, 3\pi/4 & \mu < 0, \rho > -\mu/4 \\ \phi_0 = 0, \pi/4, \pi/2, 3\pi/4 & \mu = 0, \rho > 0 \\ \phi_0 = \pm \arccos(-a/4b)/4 & \mu \neq 0, \rho < -\mu/4 \\ \phi_0 = \pi/8, 3\pi/8, 5\pi/8, 7\pi/8 & \mu = 0, \rho < 0, \end{cases} \quad (18)$$

as shown in Fig. 6. Along the line $\rho = 0$, the boundary between VBS and Néel order lies at $\mu = 0$ and is the 1D DQCP with $c = 1$ introduced in Section II A. For negative $\rho < 0$, this point splits into two transitions $\pm\mu_c$ which have \mathbb{Z}_2 symmetry breaking and where the minimum lies in between 0 and $\pi/4$. The transition lines flow to infrared Ising fixed points with $c = 1/2$ [59]. Conversely, when $\rho > 0$, a classical analysis of the potential predicts a first-order transition between AFM and VBS ground states due to the potential barrier induced by the $\cos(8\phi)$ term. These results are summarized in Fig. 7. The numerical results indicate that the sign of ρ is positive, given a strongly first-order transition is seen. It would be interesting to derive the sign of this coupling on microscopic grounds, a task which requires a full non-linear bosonization of the coupled spin-phonon system.

IV. DYNAMICAL PHONONS: SPECTRAL RESPONSE

We have numerically established the role of spin-phonon coupling on the phase diagram of the spin model. Now we turn our attention to the other side of the coin. Namely, we investigate how spin-phonon coupling affects the spectrum of phonon excitations. In the above discussion, we used an effective theory for the spin model Eq. (14) where fluctuations of the lattice modes have been integrated out. The effective model was derived in Appendix C. When we want to instead understand the properties of the phonons, we cannot take this simplifying step, but must instead study the full spin-phonon problem. Theoretically, one has to use approximate perturbative approaches to understand the effect of spin-fluctuations on the phonons. One standard method is to integrate out the spin-fluctuations, in order to derive the correction to the phonon propagator $G(q, \omega)$ [30, 38, 60]. This approach works well when one understands the behavior of the separate Hamiltonians H_s and H_p , and the spin-phonon coupling is small such that perturbation theory is controlled. The spin-model Eq. (7) has a simple phonon Green's function, given as a momentum-independent pole $G_0(q, \omega) = 1/(\omega_0^2 - \omega^2)$. Introducing a spin-phonon coupling g , this is corrected at leading order to

$$G(q, \omega) = \frac{1}{\omega_0^2 - \omega^2 - (g^2/m)\chi_D(q, \omega)}, \quad (19)$$

where $\chi_D(q, \omega)$ is the dimer-dimer correlation function of the spin-Hamiltonian H_s . Calculating these correlation functions using effective field theory [38] or scaling arguments [30] allows one to connect this result to the spin-Peierls instability; in this picture it is represented by the pole of Eq. (19) renormalizing to zero energy [61]. Additionally, the spin fluctuations cause a momentum-dependent self energy to the phonon, which can be measured experimentally as a temperature-dependent Kohn anomaly.

Following these general considerations, we return to our numerical analysis, where we will probe these effects in the full spin-phonon model. To this end, we introduce the single-particle phonon spectral function

$$A(q, \omega) = -\frac{1}{\pi} \text{Im} \int dr dt e^{i\omega t - iqr} G(r, t), \quad (20)$$

obtained as a Fourier transform of the real-space retarded Green's function

$$G(r, t) = -i\pi\theta(t) \langle \psi_0 | [a(r, t), a^\dagger(0, 0)] | \psi_0 \rangle. \quad (21)$$

We then compute $G(r, t)$ numerically by evolving the states $a^{(\dagger)}(0, 0) | \psi_0 \rangle$ in real time using the time dependent variational principle [62, 63]. We summarize details of the numerical implementation in Appendix B.

In Fig. 8 we show the phonon spectral function at various J_2/J_1 for $\omega_0 = 0.6J_1$ above the critical frequency ω_c .

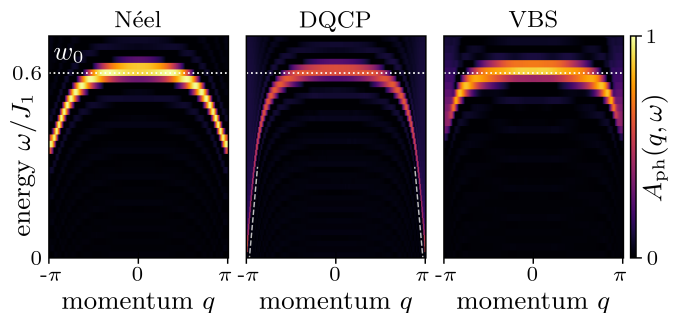


FIG. 8. **Dynamical phonon response:** Single-particle phonon spectral function $A(q, \omega)$ for parameters inside the AFM phase (left), at the DQCP (middle), and inside the VBS phase (right). The white line indicates the flat phonon band of the uncoupled model. Inside both ordered phases, the spectrum remains gapped with the flat band softening at $q = \pi$, corresponding to the ordering wavevector of the spontaneous lattice staggering. At the transition, the phonon mode softens, showing linear dispersion around $q = \pi$.

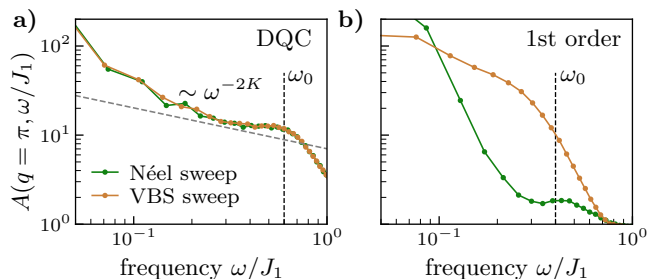


FIG. 9. **Spectral weight at the transition:** a) At the DQCP, the phonon spectral function $A(k = \pi, \omega)$ at the ordering wavevector develops a low-frequency continuum with power-law scaling $A(q = \pi, \omega) \sim \omega^{-2K}$, consistent with analytical predictions. b) Conversely, at the first-order transition, we observe a large buildup of spectral weight which triggers the lattice instability. The corresponding phonon frequencies ω_0 are marked by black dashed lines.

We take the values $J_2/J_1 \in \{0.157, 0.25733, 0.357\}$, corresponding to a ground state in the AFM phase, at the DQCP, and in the VBS phase. Inside the ordered phases, the spectral function remains gapped and the phonon band starts to soften around the ordering wavevector $q = \pi$. We interpret this as a Kohn anomaly of the phonon dispersion due to large fluctuations of VBS order in the spin chain. We symmetrize the spectrum in the VBS phase to reduce numerical artifacts due to the two-site unit cell, see details in Appendix B.

At the transition, the phonons become gapless and a soft mode emerges at $q = \pi$, where the spectral weight of this mode is spread out into a weak continuum at low energies. We plot the frequency dependence of this continuum on a logarithmic axes $A(q = \pi, \omega)$ and compare it to a power-law in Fig. 9a. For frequencies $\omega < \omega_0$, the numerical data is in good agreement with the critical scaling $A(q = \pi, \omega) \sim \omega^{-2K}$. This is consistent with the

low-energy scaling of dimer-dimer correlations, $\chi_D(q = \pi, \omega) \sim \omega^{-2K}$, and agrees with the perturbative correction to the phonon Green's function in Eq. (19). The low-frequency behaviour of the phonon spectral function shows a complete breakdown of the quasiparticle picture around this momentum $q = \pi$. Instead, the phonons hybridize with the critical VBS fluctuations at the DQCP, showing signs of fractionalization in their dynamical response [30, 60]. Deviations from the power-law behavior appear at very small frequencies, which we attribute to the finite time cutoff imposed by the maximal simulation time.

For comparison, we also show the corresponding spectral weight at the first-order transition for $\omega_0 = 0.4J_1$ in in Fig. 9b. There, we observe a significant buildup of spectral weight at low frequencies, which triggers the lattice instability. This is consistent with the perturbative description of a spin-Peierls instability being due to phonon condensation [38] and the understanding of the first-order transition as a spin-Peierls instability of the DQCP [32]. Additionally, there is a significant difference in weight between preparing the ground state with a sweep from the AFM and VBS phase, respectively, which we attribute to reaching distinct coexistence regimes upon approaching the transition.

V. DISCUSSION & OUTLOOK

In this work, we have determined the phase diagram of a prototypical example of 1D DQC coupled to lattice vibrations. We numerically confirm the stability of DQC for phonon frequencies above a critical threshold, as predicted by Ref. [32]. We demonstrate that the main consequence of spin-lattice coupling is a reduction of the Luttinger parameter K . The breakdown of DQC is then caused by an additional symmetry allowed $\cos(8\phi)$ term arising from higher-order bosonization.

The phenomenology of the transition below the critical phonon frequency depends on the sign of the $\cos(8\phi)$ term. Numerical results indicate a negative prefactor, which introduces a potential barrier at the transition and results in a strong first-order transition. Conversely, with a positive prefactor, the theory is expected to describe the critical line of the Ashkin-Teller model consisting of two Ising transitions instead. The analogy to the high-symmetry critical point of the Ashkin-Teller model allows us to predict that the critical endpoint lies in the four-state Potts universality class.

Our results are directly applicable to a broad class of 1D systems hosting DQC coupled to appropriate lattice degrees of freedom, as many such models are described by the same effective low-energy theory. They further complement recent studies predicting analogous lattice instabilities in 2D spin liquids [30, 31] and at a 2D incarnation of DQC [32, 33]. Notably, 1D systems hosting DQC offer a natural platform [24] to realize and probe Ashkin-Teller type physics along the line of continuous

DQC. An interesting question is whether lattice instabilities also arise at DQCPs that do not involve translation symmetry breaking, given that the lattice coupling can still lower the relevant Luttinger parameter. Long-range 1D spin chains with easy-axis anisotropy provide a possible setting in this direction, as they have been argued to enable continuous breaking of the U(1) spin-rotation symmetry [64]. Such models can therefore host transitions between ordered phases breaking distinct spin symmetries. Another example is the direct x-FM to z-FM transition in Ref. [21], where the effective theory is of BKT type, rendering the presence of a corresponding instability *a priori* unclear.

An advantage of the 1D setting is that quasi-exact numerical results $A(q = \pi, \omega) \sim \omega^{-2K}$ can be obtained for the critical scaling of the phonon spectral function along the DQC line. Similar scaling behavior has recently been explored in the context of spin liquids [65], and is expected to extend to the 2D case of DQC as well. In the low-temperature regime $\beta \gg \omega_0$, the phonon spectral function is directly related to the structure factor $S(q, \omega) \approx A(q, \omega)$ via the fluctuation-dissipation theorem [66]. The latter is experimentally accessible via inelastic neutron scattering [67–69], providing a direct experimentally accessible route to investigate lattice driven breakdown of DQC. In this context, it is worth noting that experiments on $\text{SrCu}_2(\text{BO}_3)_2$ have reported a direct AFM-VBS transition whose character changes with pressure [70, 71]. Our results highlight that further theoretical work is also needed into understanding the phase diagrams of 2D realizations of DQC with spin-phonon coupling, given the effect of pressure in modifying phonon energy scales.

On a technical level, an interesting further direction is to derive the sign of the $\cos(8\phi)$ term from microscopics, by performing a full non-linear bosonization of the coupled spin-phonon system. Given that the sign of the relevant $\cos(8\phi)$ term is in principle tunable by adding additional symmetry-conserving 8-fermion terms, one may also explore the possibility of an intermediate coexistence phase analog to the conventional Ashkin-Teller model. This requires to identify an operator that introduces a strong $\cos(8\phi)$ term, while simultaneously keeping the $\cos(4\phi)$ term stable. As a result, DQC would not be destroyed by the usual first order transition but rather by turning into a split transition with an intermediate phase. Amusingly, the resulting phase diagram would resemble the generic Ginzburg-Landau behavior albeit with a very different origin. Understanding such an unusual instability of DQC beyond the one-dimensional settings will be a formidable task for future numerics and analytics.

ACKNOWLEDGMENTS

We gratefully acknowledge discussions with Johannes Hauschild, Lukas Janssen, Urban Seifert, and Manuel Weber. We acknowledge support from the

Deutsche Forschungsgemeinschaft (DFG, German Research Foundation) under Germany's Excellence Strategy—EXC–2111–390814868, TRR 360 – 492547816 and DFG grants No. KN1254/1-2, KN1254/2-1, the European Union (grant agreement No 101169765), as well as the Munich Quantum Valley, which is supported by the Bavarian state government with funds from the Hightech Agenda Bayern Plus.

DATA AVAILABILITY

Numerical data and codes that support the findings of this article are available on Zenodo and from the authors upon reasonable request [72].

-
- [1] T. Senthil, A. Vishwanath, L. Balents, S. Sachdev, and M. P. Fisher, Deconfined quantum critical points, *Science* **303**, 1490 (2004).
- [2] T. Senthil, L. Balents, S. Sachdev, A. Vishwanath, and M. P. Fisher, Quantum criticality beyond the landau-ginzburg-wilson paradigm, *Physical Review B—Condensed Matter and Materials Physics* **70**, 144407 (2004).
- [3] L. D. Landau and E. M. Lifshitz, *Statistical physics: volume 5*, Vol. 5 (Elsevier, 2013).
- [4] K. G. Wilson and J. Kogut, The renormalization group and the ϵ expansion, *Physics reports* **12**, 75 (1974).
- [5] Y. Liu, Z. Wang, T. Sato, M. Hohenadler, C. Wang, W. Guo, and F. F. Assaad, Superconductivity from the condensation of topological defects in a quantum spin-hall insulator, *Nature Communications* **10**, 2658 (2019).
- [6] E. Khalaf, S. Chatterjee, N. Bultinck, M. P. Zaletel, and A. Vishwanath, Charged skyrmions and topological origin of superconductivity in magic-angle graphene, *Science advances* **7**, eabf5299 (2021).
- [7] M. Christos, S. Sachdev, and M. S. Scheurer, Superconductivity, correlated insulators, and wess–zumino–witten terms in twisted bilayer graphene, *Proceedings of the National Academy of Sciences* **117**, 29543 (2020).
- [8] M. Christos, L. Shackleton, S. Sachdev, and Z.-X. Luo, Deconfined quantum criticality of nodal d-wave superconductivity, néel order, and charge order on the square lattice at half-filling, *Physical Review Research* **6**, 033018 (2024).
- [9] Z. H. Liu, M. Vojta, F. F. Assaad, and L. Janssen, Metallic and deconfined quantum criticality in dirac systems, *Physical Review Letters* **128**, 087201 (2022).
- [10] Y.-H. Zhang and S. Sachdev, Deconfined criticality and ghost fermi surfaces at the onset of antiferromagnetism in a metal, *Physical Review B* **102**, 155124 (2020).
- [11] A. Nikolaenko, J. von Milczewski, D. G. Joshi, and S. Sachdev, Spin density wave, fermi liquid, and fractionalized phases in a theory of antiferromagnetic metals using paramagnons and bosonic spinons, *Physical Review B* **108**, 045123 (2023).
- [12] A. Götz, M. Hohenadler, and F. F. Assaad, Phases and exotic phase transitions of a two-dimensional suschrieffer-heeger model, *Physical Review B* **109**, 195154 (2024).
- [13] Y. Liu, T. Sato, D. Hou, Z. Wang, W. Guo, and F. F. Assaad, Edge modes of topological mott insulators and deconfined quantum critical points, [arXiv:2508.04455](https://arxiv.org/abs/2508.04455) (2025).
- [14] X. Chen, S. Liu, D.-c. Lu, and N. Tantivasadakarn, Spontaneous breaking of non-invertible symmetries and duality to beyond-landau transitions, [arXiv:2605.27672](https://arxiv.org/abs/2605.27672) (2026).
- [15] M. Weber, [Competing dirac masses in one dimension: Symmetry-enhanced pseudo-first-order transition and deconfined criticality](https://arxiv.org/abs/2508.04455) (2025).
- [16] M. Levin and T. Senthil, Deconfined quantum criticality and néel order via dimer disorder, *Physical Review B—Condensed Matter and Materials Physics* **70**, 220403 (2004).
- [17] T. Senthil and M. P. Fisher, Competing orders, nonlinear sigma models, and topological terms in quantum magnets, *Physical Review B—Condensed Matter and Materials Physics* **74**, 064405 (2006).
- [18] A. Nahum, P. Serna, J. Chalker, M. Ortuño, and A. Somoza, Emergent so(5) symmetry at the néel to valence-bond-solid transition, [arXiv:1508.06668](https://arxiv.org/abs/1508.06668) (2015).
- [19] C. Wang, A. Nahum, M. A. Metlitski, C. Xu, and T. Senthil, Deconfined quantum critical points: symmetries and dualities, *Physical Review X* **7**, 031051 (2017).
- [20] S. Jiang and O. Motrunich, Ising ferromagnet to valence bond solid transition in a one-dimensional spin chain: Analogies to deconfined quantum critical points, *Physical Review B* **99**, 075103 (2019).
- [21] B. Roberts, S. Jiang, and O. I. Motrunich, Deconfined quantum critical point in one dimension, *Physical Review B* **99**, 165143 (2019).
- [22] T. Giamarchi, *Quantum physics in one dimension*, Vol. 121 (Clarendon press, 2003).
- [23] C. Mudry, A. Furusaki, T. Morimoto, and T. Hikihara, Quantum phase transitions beyond landau-ginzburg theory in one-dimensional space revisited, *Physical Review B* **99**, 205153 (2019).
- [24] J. Y. Lee, J. Ramette, M. A. Metlitski, V. Vuletić, W. W. Ho, and S. Choi, Landau-forbidden quantum criticality in rydberg quantum simulators, *Physical review letters* **131**, 083601 (2023).
- [25] A. Romen, S. Birnkammer, and M. Knap, Deconfined quantum criticality in the long-range, anisotropic heisenberg chain, *SciPost Physics Core* **7**, 008 (2024).
- [26] E. Pytte, Peierls instability in heisenberg chains, *Physical Review B* **10**, 4637 (1974).
- [27] R. E. Peierls, *Quantum theory of solids* (Oxford university press, 1955).
- [28] M. Cross and D. S. Fisher, A new theory of the spin-peierls transition with special relevance to the experiments on ttfcubdt, *Physical Review B* **19**, 402 (1979).
- [29] P. Pincus, Instability of the uniform antiferromagnetic chain, *Solid State Communications* **9** (1971).
- [30] U. F. P. Seifert, J. Willsher, M. Drescher, F. Pollmann, and J. Knolle, Spin-Peierls instability of the U(1) Dirac spin liquid, *Nature Communications* **15**, 7110 (2024).

- [31] F. Ferrari, J. Willsher, U. F. Seifert, R. Valentí, and J. Knolle, Stability of algebraic spin liquids coupled to quantum phonons, *Physical Review Research* **7**, L042053 (2025).
- [32] D. Hofmeier, J. Willsher, U. F. P. Seifert, and J. Knolle, Spin-peierls instability of deconfined quantum critical points, *Physical Review B* **110** (2024).
- [33] A. Götz, F. F. Assaad, and N. C. Costa, Tuning the order of a deconfined quantum critical point, [arXiv:2412.17215](https://arxiv.org/abs/2412.17215) (2024).
- [34] J. Ashkin and E. Teller, Statistics of two-dimensional lattices with four components, *Physical Review* **64**, 178 (1943).
- [35] M. Kohmoto, M. den Nijs, and L. P. Kadanoff, Hamiltonian studies of the $d=2$ ashkin-teller model, *Physical Review B* **24**, 5229 (1981).
- [36] Y. Aoun, M. Dober, and A. Glazman, Phase diagram of the ashkin-teller model, *Communications in Mathematical Physics* **405**, 37 (2024).
- [37] W. Kohn, Image of the fermi surface in the vibration spectrum of a metal, *Physical Review Letters* **2**, 393 (1959).
- [38] A. Luther and I. Peschel, Single-particle states, Kohn anomaly, and pairing fluctuations in one dimension, *Physical Review B* **9**, 2911 (1974).
- [39] S. R. White, Density matrix formulation for quantum renormalization groups, *Physical review letters* **69**, 2863 (1992).
- [40] U. Schollwöck, The density-matrix renormalization group in the age of matrix product states, *Annals of physics* **326**, 96 (2011).
- [41] J. Hauschild, J. Unfried, S. Anand, B. Andrews, M. Bintz, U. Borla, S. Divic, M. Drescher, J. Geiger, M. Hefel, *et al.*, Tensor network python (tenpy) version 1, *SciPost Physics Codebases* , 041 (2024).
- [42] G. Vidal, Efficient classical simulation of slightly entangled quantum computations, *Physical review letters* **91**, 147902 (2003).
- [43] G. Vidal, Classical simulation of infinite-size quantum lattice systems in one spatial dimension, *Physical review letters* **98**, 070201 (2007).
- [44] D. Perez-Garcia, F. Verstraete, M. M. Wolf, and J. I. Cirac, Matrix product state representations, [arXiv:quant-ph/0608197](https://arxiv.org/abs/quant-ph/0608197) (2006).
- [45] R. J. Glauber, Coherent and incoherent states of the radiation field, *Physical Review* **131**, 2766 (1963).
- [46] E. Orignac and R. Chitra, Mean-field theory of the spin-Peierls transition, *Physical Review B* **70**, 214436 (2004).
- [47] R. Citro, E. Orignac, and T. Giamarchi, Adiabatic-antiadiabatic crossover in a spin-Peierls chain, *Physical Review B* **72**, 024434 (2005).
- [48] F. Pollmann, S. Mukerjee, A. M. Turner, and J. E. Moore, Theory of finite-entanglement scaling at one-dimensional quantum critical points, *Physical review letters* **102**, 255701 (2009).
- [49] K. Vollmayr, J. D. Reger, M. Scheucher, and K. Binder, Finite size effects at thermally-driven first order phase transitions: A phenomenological theory of the order parameter distribution, *Zeitschrift für Physik B Condensed Matter* **91**, 113 (1993).
- [50] L. P. Kadanoff, Singularities near the bifurcation point of the Ashkin-Teller model, *Physical Review B* **22**, 1405 (1980).
- [51] G. Mussardo, V. Riva, and G. Sotkov, Semiclassical particle spectrum of double sine-gordon model, *Nuclear Physics B* **687**, 189–219 (2004).
- [52] G. Takács and F. Wágner, Double sine-gordon model revisited, *Nuclear Physics B* **741**, 353–367 (2006).
- [53] R. Mouland, D. Tong, and B. Zan, Phases of 2d gauge theories and symmetric mass generation, [arXiv:2509.12305](https://arxiv.org/abs/2509.12305) (2025).
- [54] L. Tagliacozzo, T. R. de Oliveira, S. Iblisdir, and J. I. Latorre, Scaling of entanglement support for matrix product states, *Physical Review B—Condensed Matter and Materials Physics* **78**, 024410 (2008).
- [55] I. Enting, Critical exponents for the four-state potts model, *Journal of Physics A: Mathematical and General* **8**, L35 (1975).
- [56] R. B. Pearson, Conjecture for the extended potts model magnetic eigenvalue, *Physical Review B* **22**, 2579 (1980).
- [57] B. Nienhuis, Critical behavior of two-dimensional spin models and charge asymmetry in the coulomb gas, *Journal of Statistical Physics* **34**, 731 (1984).
- [58] M. P. den Nijs, A relation between the temperature exponents of the eight-vertex and q-state potts model, *Journal of Physics A: Mathematical and General* **12**, 1857 (1979).
- [59] G. Delfino and P. Grinza, Universal ratios along a line of critical points. the Ashkin-Teller model, *Nuclear Physics B* **682**, 521 (2004), [arXiv:hep-th/0309129](https://arxiv.org/abs/hep-th/0309129).
- [60] J. Y. Lee, Y.-Z. You, S. Sachdev, and A. Vishwanath, Signatures of a Deconfined Phase Transition on the Shastry-Sutherland Lattice: Applications to Quantum Critical SrCu₂(BO₃)₂, *Physical Review X* **9**, 041037 (2019).
- [61] J. Willsher, *Dynamics and Stability of Critical Spin Liquids*, Ph.D. thesis, Technische Universität München (2025), available at <https://mediatum.ub.tum.de/?id=1785165>.
- [62] J. Haegeman, J. I. Cirac, T. J. Osborne, I. Pižorn, H. Verschelde, and F. Verstraete, Time-dependent variational principle for quantum lattices, *Physical Review Letters* **107**, 070601 (2011).
- [63] J. Haegeman, C. Lubich, I. Oseledets, B. Vandereycken, and F. Verstraete, Unifying time evolution and optimization with matrix product states, *Physical Review B* **94**, 165116 (2016).
- [64] M. F. Maghrebi, Z.-X. Gong, and A. V. Gorshkov, Continuous symmetry breaking in 1d long-range interacting quantum systems, *Physical Review Letters* **119**, 023001 (2017).
- [65] J. Willsher and J. Knolle, Dynamics and stability of U(1) spin liquids beyond mean-field theory: Triangular-lattice J1-J2 Heisenberg model, [arXiv:2503.13831](https://arxiv.org/abs/2503.13831) (2025).
- [66] G. D. Mahan, *Many-particle physics* (Springer Science & Business Media, 2013).
- [67] G. L. Squires, *Introduction to the theory of thermal neutron scattering* (Courier Corporation, 1996).
- [68] G. Shirane, S. M. Shapiro, and J. M. Tranquada, *Neutron scattering with a triple-axis spectrometer: basic techniques* (Cambridge University Press, 2002).
- [69] B. T. M. Willis and C. J. Carlile, *Experimental neutron scattering* (Oxford University Press, 2017).
- [70] Y. Cui, L. Liu, H. Lin, K.-H. Wu, W. Hong, X. Liu, C. Li, Z. Hu, N. Xi, S. Li, *et al.*, Proximate deconfined quantum critical point in srCu₂(bo₃)₂, *Science* **380**, 1179 (2023).
- [71] J. Guo, P. Wang, C. Huang, B.-B. Chen, W. Hong, S. Cai, J. Zhao, J. Han, X. Chen, Y. Zhou, *et al.*, Deconfined quantum critical point lost in pressurized srCu₂

- (bo3) 2, *Communications Physics* **8**, 75 (2025).
- [72] All data and simulation codes are available upon reasonable request at <https://doi.org/10.5281/zenodo.20037182>.
- [73] S. R. White, Density matrix renormalization group algorithms with a single center site, *Physical Review B—Condensed Matter and Materials Physics* **72**, 180403 (2005).
- [74] H. N. Phien, G. Vidal, and I. P. McCulloch, Infinite boundary conditions for matrix product state calculations, *Physical Review B—Condensed Matter and Materials Physics* **86**, 245107 (2012).
- [75] A. Milsted, J. Haegeman, T. J. Osborne, and F. Verstraete, Variational matrix product ansatz for nonuniform dynamics in the thermodynamic limit, *Physical Review B—Condensed Matter and Materials Physics* **88**, 155116 (2013).
- [76] S. R. White and I. Affleck, Spectral function for the $s=1$ heisenberg antiferromagnetic chain, *Physical Review B—Condensed Matter and Materials Physics* **77**, 134437 (2008).
- [77] H. Knops and L. Den Ouden, Momentum space renormalization for the sine-gordon model, *Physica A: Statistical Mechanics and its Applications* **103**, 597 (1980).
- [78] P. Nozieres and F. Gallet, The roughening transition of crystal surfaces. i. static and dynamic renormalization theory, crystal shape and facet growth, *Journal de physique* **48**, 353 (1987).

Appendix A: Bosonization of 1D spin models

In this appendix, we briefly recapitulate the standard bosonization procedure for the sine-Gordon action in Eq. (3) as found, e.g., in [22].

First, the spin operators are fermionized using a Jordan-Wigner transformation

$$\begin{aligned} S_j^z &= c_j^\dagger c_j - \frac{1}{2}, \\ S_j^+ &= c_j^\dagger \exp\left(i\pi \sum_{k<j} c_k^\dagger c_k\right), \\ S_j^- &= c_j \exp\left(i\pi \sum_{k<j} c_k^\dagger c_k\right), \end{aligned} \quad (\text{A1})$$

with a subsequent transformation $c_j \rightarrow (-1)^j c_j$ to bring the antiferromagnetic spin Hamiltonian into the fermion Hamiltonian

$$\begin{aligned} H_s &= -\frac{J_1}{2} \sum_j \left[(c_{j+1}^\dagger c_j + c_j^\dagger c_{j+1}) \right. \\ &\quad \left. - 2\Delta (c_j^\dagger c_j - \frac{1}{2})(c_{j+1}^\dagger c_{j+1} - \frac{1}{2}) \right] \\ &+ \frac{J_2}{2} \sum_j \left[(c_{j+2}^\dagger c_j + c_j^\dagger c_{j+2})(1 - 2c_{j+1}^\dagger c_{j+1}) \right. \\ &\quad \left. + 2\Delta (c_{j+2}^\dagger c_{j+2} - \frac{1}{2})(c_j^\dagger c_j - \frac{1}{2}) \right]. \end{aligned} \quad (\text{A2})$$

Next, the continuum limit

$$\sum_j \longrightarrow \frac{1}{a} \int dx, \quad c_j \longrightarrow \sqrt{a} \psi(x_j) \quad (\text{A3})$$

is taken and the resulting Hamiltonian is bosonized by splitting the oscillating fermionic field into left and right moving fermions according to

$$\begin{aligned} \psi(x) &= e^{ik_F x} \psi_R(x) + e^{-ik_F x} \psi_L(x) \\ \psi_{L[R]} &= \frac{1}{\sqrt{2\pi\gamma}} e^{-[+i\phi(x) - i\theta(x)]} \end{aligned} \quad (\text{A4})$$

that admit a low-energy expansion into bosonic modes. Here, we introduced the UV lattice cutoff γ of the low-energy expansion. For the antiferromagnetic spin model, the fermions are at half filling $k_F = \pi/(2a)$. One subsequently inserts Eq. (A4) into Eq. (A2) and keeps only non oscillating terms to bring the Hamiltonian into the sine-Gordon form of Eq. (3). The four-fermion terms contribute to the $\cos(4\phi)$ term. Specifically,

$$\begin{aligned} J_1 \Delta c_j^\dagger c_j c_{j+1}^\dagger c_{j+1} &\rightarrow -2J_1 \Delta \cos(4\phi) \\ -J_2 (c_{j+2}^\dagger c_j + c_j^\dagger c_{j+2})(c_{j+1}^\dagger c_{j+1}) &\rightarrow 4J_2 \cos(4\phi) \\ J_2 \Delta c_{j+2}^\dagger c_{j+2} c_j^\dagger c_j &\rightarrow 2J_2 \Delta \cos(4\phi), \end{aligned} \quad (\text{A5})$$

from which $\mu = 2J_1 \Delta - 2J_2(2 + \Delta)$ is recovered up to prefactors including the lattice spacing a and UV lattice cutoff γ , see e.g. Ref. [23] for the detailed derivation. Tuning J_2 can induce a sign change of μ which describes the DQCP of the spin model.

Appendix B: Numerical implementation

All simulations are performed using the TeNPy library [41]. We explicitly enforce conservation of the total spin-z component $\sum_j S_j^z$. We implement the Hamiltonian in Eq. (2) with one spin-1/2 per site and the Hamiltonian of the spin-phonon model in Eq. (1) as a chain of alternating spin-1/2 and boson sites. For the spin model, it suffices to consider bond dimensions $\chi_s \leq 220$, whereas for the spin-phonon model, we consider bond dimensions up to $\chi = 472$.

We implement a sweep protocol to capture the transition. The primary advantage is improved convergence close to the critical point. In addition, the protocol induces controlled hysteresis near criticality, which can be used to obtain a precise estimate of the critical point, as outlined below. We first initialize a trial MPS $|\psi_0\rangle$ in the fully polarized Néel state or a chain of singlets on neighboring bonds and compute the ground state for some value of J_2 deep inside the corresponding ordered phase. We use the infinite system variant of the Density Matrix Renormalization Group (DMRG) implemented within the TeNPy library [41].

In each step, we approach the transition by slightly varying J_2/J_1 and reuse the previous variational ground state as initial state for the subsequent simulation. *Crucially*, we recycle the final left and right environment of the previous simulation as initial environment for the subsequent run. These environments correspond to the left and right infinite half chain. Within the DMRG protocol, we insert an additional unit cell into these environments after each sweep. In particular, this means that the "current" Hamiltonian is only implemented on a window $L_{\text{cell}} \cdot N_{\text{sweeps}}$, with $L_{\text{cell}} = 16$. To ensure that simulations are converged, we insert at least $N \approx \xi_{\text{max}}$ sites into each environment in each step and vary J_2/J_1 slower, when close to the transition. The main advantage of this approach is that it gives better control over the order parameter residuals discussed in the main text.

In the spin-phonon model, local DMRG updates act on a single spin site. This leads to a reduces buildup of entanglement upon approaching the transition. To circumvent this problem, we introduce a small density mixer [73] with initial amplitude $a_0 = 10^{-5}$ that exponentially decays to a final amplitude $a_f = 10^{-8}$ over 20 steps *in each simulation*. The strength of the mixer is tuned to generate sufficient entanglement, while allowing for sufficient hysteresis close to the critical point.

A precise estimate of the critical point J_{2c}/J_1 is found using a variant of the method introduced in Ref. [21]. At finite bond dimension χ , an MPS does not capture

the correct second-order phase transition, but instead exhibits a weakly first-order phase transition at a pseudocritical point $J_{2c}(\chi)/J_1$ that shifts with χ . Due to hysteresis in sweep protocols, simulations near the transition converge to a metastable state on the opposite side of the initial phase rather than the correct ground state, resulting in a level crossing. In Ref. [21], the critical point is estimated from this level crossing via the zero crossing of $\Delta E \equiv E_{VBS}(J_2) - E_{AFM}(J_2)$, where E_* denotes the variational energy of a sweep originating in the respective phase.

In our simulations, ΔE becomes unstable at large bond dimensions. Instead, we determine a critical point for each sweep separately by fitting the energy linearly on both sides of the transition (identified via the order parameters), with $J_{2c,AFM}(VBS)/J_1$ given by the intersection. Due to hysteresis, we find $J_{2c,AFM}(\chi) > J_{2c,VBS}(\chi)$. Both estimates show negligible drift with χ and differ by $J_{2c,AFM}(\chi) - J_{2c,VBS}(\chi) \lesssim 4 \cdot 10^{-4} J_1$. We can therefore take

$$J_{2c} = 1/N_\chi \sum_\chi \frac{1}{2} (J_{2c,AFM}(\chi) + J_{2c,VBS}(\chi)) \quad (\text{B1})$$

as our final estimate. We summarize the method in Fig. 10.

We implement dynamical phonons as bosons, Eq. (8), and truncate the local Hilbert space to at most $N_{\max} = 6$ phonons per site for computational feasibility. Here, we briefly justify this approximation. For small ω_0 , the dominant phonon energy scale is given by the spin-phonon coupling $a_j^\dagger + a_j$, and the phonon state is expected to be close to some coherent state $|\alpha\rangle = e^{-|\alpha|^2/2} \sum_{n=0}^{\infty} \alpha^n / \sqrt{n!} |n\rangle$. At any finite ω_0 , the average occupation $\langle n_j \rangle = \langle a_j^\dagger a_j \rangle$ remains finite and we expect the state to have maximal weight around $|\alpha|^2 \approx \langle n_j \rangle$, with exponentially suppressed tails at large enough $n \gg |\alpha|^2$. Additionally, $\langle n_j \rangle$ decreases upon increasing ω_0 . Numerically, we find $\langle n_j \rangle \lesssim 0.33$ and $\langle \psi_{gs} | n_j = 6 \rangle \langle n_j = 6 | \psi_{gs} \rangle \lesssim 5 \cdot 10^{-6}$ for frequencies $\omega_0 \geq 0.4$, hence even well inside the first-order regime, justifying the truncation. We further confirm numerically that the relevant physical behavior is unchanged even in the first order regime when tuning the phonon cutoff (where truncation is most significant), see Fig. 11.

The phonon spectral function is given by $A(q, \omega) = -1/\pi \text{Im}(G(q, \omega))$, where $G(q, \omega)$ denotes the Fourier transform of the retarded Green's function

$$G(r, t) = -i\pi\theta(t) \langle \psi_0 | [a(r, t), a^\dagger(0, 0)] | \psi_0 \rangle. \quad (\text{B2})$$

Here, we assume time-translation invariance and translational invariance of the ground state $|\psi_0\rangle$. In the VBS phase, the latter is broken. In principle, this requires computing the Green's function separately for each sublattice of the enlarged two-site unit cell. Owing to the substantial cost of the numerical simulations, we restrict the analysis to applying the first operator only on the

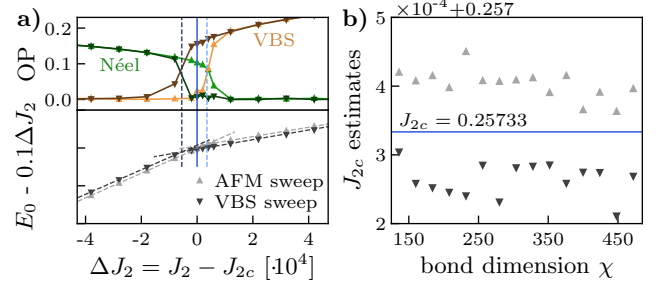


FIG. 10. a) We obtain a precise estimate of the critical point J_{2c} by performing separate linear fits of ground state energy E_0 on both sides of the transition for each sweep direction, thereby obtaining two independent estimates $J_{2c,AFM}(\chi)$ and $J_{2c,VBS}(\chi)$ for each bond dimensions χ . b) The estimates $J_{2c,AFM}(\chi)$ (light gray) and $J_{2c,VBS}(\chi)$ (dark gray) show minimal drift with bond dimension, allowing us to take the arithmetic mean as final estimate for the critical point J_{2c} .

first site of the unit cell and subsequently evaluate correlations with operators on both sublattices. Because the VBS ground state breaks translation invariance only by staggering, correlations between the sublattices differ only by a factor (-1) . Therefore this approximation produces the correct results, even though the spectral function inside the VBS phase is not translation symmetric in real space.

We compute the retarded Green's function numerically using the time-dependent variational principle (TDVP) [62, 63]. The initial operator is applied at the center of the chain, and correlations are evaluated for all sites of the chain by applying the second operator and computing the overlap with the unevolved ground state at regular intervals $\delta t = 0.2/J_1$, up to a maximal time $t_m \approx 80/J_1$.

To eliminate finite-size effects, we use a hybrid approach in which time evolution is performed on an MPS segment with $L = 256$ phonon sites embedded in two infinite half chains [74, 75]. The MPS segment is obtained by repeating the unit cell and the boundary environments are given by the dominant left and right eigenvector of the MPO transfer matrix up to an extensive energy contribution. These environments can be efficiently computed using the method introduced in Ref. [74]. We use the 2-site version of TDVP which allows the bond dimension to increase over time. We start from the ground state with bond dimension $\chi = 400$ and limit the maximal bond dimension of the subsequent time evolution to $\chi = 600$.

We subsequently use linear prediction [76] to extrapolate the correlations $G(r, t)$ up to twice the original simulation time. We then apply a Gaussian window function $e^{-t^2/(2\sigma^2 \cdot 4t_m^2)}$ with $\sigma = 0.25$ to reduce Gibbs ringing. Applying this window changes the scaling of the spectral weight according to

$$A_{\text{total}}(q, \omega) = A(q, \omega) \star \hat{f}(\omega), \quad (\text{B3})$$

where \star denotes the convolution and $\hat{f}(\omega) \equiv$

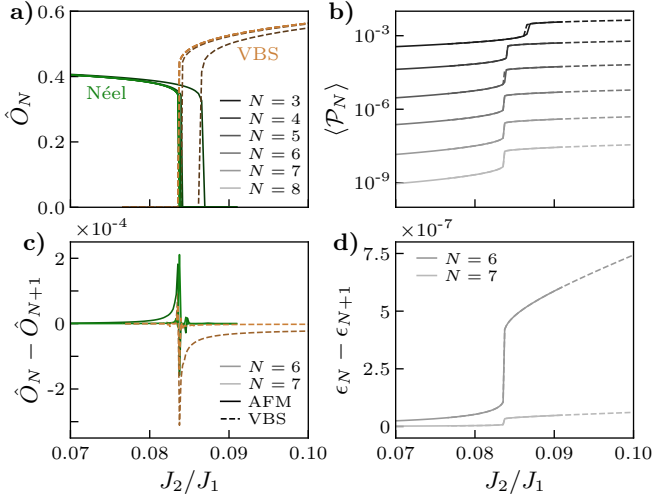


FIG. 11. Effects of the phonon cutoff N . Results are shown for $\omega_0 = 0.4$, well within the 1st-order regime. a) The location of the critical point remains unchanged for $N \geq 5$. b) The order parameters differ by $\hat{O}_N - \hat{O}_{N+1} \leq 3 \cdot 10^{-4}$, corresponding to a relative deviation $\delta\hat{O}/\hat{O} \leq 10^{-3}$. c) The ground state exhibits exponentially small overlap with configurations containing more than $N \geq 3$ phonons per bond, measured via the projector $\mathcal{P}_N \equiv |n_j = N\rangle \langle n_j = N|$. d) Near the transition, the variational ground-state energy varies only slightly with increasing cutoff N . Notably, the discontinuity in the ground-state energy in the first-order regime exceeds this variation by several orders of magnitude.

$\sqrt{\pi\sigma^2 t_m^2} e^{-\pi^2\omega^2\sigma^2 t_m^2}$ is the Fourier transform of the Gaussian window function. The frequency broadening arising from this gaussian window is $\delta\omega = \frac{1}{\pi\sigma t_m} \approx 0.008J_1$.

Appendix C: Effective sine-Gordon theory for dynamical phonons

Here, we reproduce results from Ref. [32] for the low-energy effective theory of the spin-phonon model in Eq. (1) in the large phonon frequency limit $\omega_0 \rightarrow \infty$. If we include temporal fluctuations of the field u_j , the combined action of spins and phonons reads

$$S(\omega_0) = S_{\text{SG}} + \int dx d\tau \left\{ \frac{\rho}{2} [|\partial_\tau u|^2 + \omega_0^2 |u|^2] + 2gu \sin(2\phi) \right\} \quad (\text{C1})$$

with phonon mass density $\rho = m/a$ and spin-phonon coupling strength g . Integrating out the quadratic displacement field yields

$$S = S_{\text{SG}} + g^2 \int dx d\tau d\tau' G(\tau - \tau') \quad (\text{C2})$$

$$\times [\cos(2\phi_\tau + 2\phi_{\tau'}) - \cos(2\phi_\tau - 2\phi_{\tau'})]. \quad (\text{C3})$$

with the phonon propagator

$$G_{\omega_0}(\tau - \tau') = \frac{1}{2m\omega_0} e^{-\omega_0|\tau - \tau'|}. \quad (\text{C4})$$

In the limit $\omega_0 \rightarrow \infty$ the propagator is completely local in space and time. Thus, for large ω_0 , we can Taylor expand the cosine terms which depend on $\phi(\tau), \phi(\tau')$ [32]. The expansion of the sum reads

$$\cos\{2[\phi(\tau) + \phi(\tau')]\} = \cos[4\phi(\tau)] \quad (\text{C5})$$

$$-2\Delta\tau\partial_\tau\phi\sin(4\phi(\tau)) - (\Delta\tau)^2\partial_\tau^2\phi\sin[4\phi(\tau)] \quad (\text{C6})$$

$$-2(\Delta\tau)^2(\partial_\tau\phi)^2\cos[4\phi(\tau)] \quad (\text{C7})$$

The term $\partial_\tau\phi\sin(4\phi)$ becomes relevant at $K < 1/4$, but constitutes only a total derivative $\partial_\tau\phi\sin(4\phi) \sim \partial_\tau\cos(4\phi)$ and hence describes boundary effects which we may ignore in the thermodynamic limit. The next higher derivative terms have scaling dimension $2 + 4K$ and are thus irrelevant over the whole considered regime. Inserting this back into the action Eq. (C3) renormalizes the prefactor of the $\cos(4\phi)$ term

$$\mu' = \mu + \frac{g^2}{\rho\omega_0^2} \quad (\text{C8})$$

implying that the DQCP simply gets shifted from $\mu = 0$ to $\mu_c = -g^2/(\rho\omega_0)^2$.

In order to Taylor expand the difference, one has to normal order first. Using the identity [77, 78]

$$\cos(\phi) =: \cos(\phi) : e^{-\langle\phi^2\rangle_0/2} \quad (\text{C9})$$

and using the standard result $\langle[\phi(\tau) - \phi(\tau')]^2\rangle_0 = K \log|\tau - \tau'|$ [22], one has to leading order

$$\cos\{2[\phi(\tau) - \phi(\tau')]\} = \left\{ 1 - 2(\tau - \tau')^2 [\partial_\tau\phi(\tau)]^2 \right\} |\tau - \tau'|^{-2K} \quad (\text{C10})$$

which after performing the τ' integration renormalizes the Luttinger parameter $K' = \gamma K < K$

$$\gamma = \left(\frac{2\pi K g^2 \Gamma(3 - 2K)}{\rho\omega_0^{4-2K}} + 1 \right)^{-1/2} \quad (\text{C11})$$

where $\Gamma(x)$ denotes the Euler gamma function.

The new theory is of the same form as the original sine-Gordon action (3),

$$S_{\text{SG}'} = \int dx d\tau \left[\frac{1}{2\pi K'} (\gamma(\partial_x\phi)^2 + \gamma^{-1}(\partial_\tau\phi)^2) - \mu' \cos(4\phi) \right]. \quad (\text{C12})$$

but with renormalized parameters

$$K' = \gamma K, \quad \mu' = \mu + g^2/(\rho\omega_0^2) \quad (\text{C13})$$

and hosts a line of DQCP as long as $K' > 1/8$. Solving for $\gamma K = 1/8$, we obtain

$$\rho\omega_c^{4-2K} = \frac{2\pi K \Gamma(3 - 2K)}{64K^2 - 1} g^2 \quad (\text{C14})$$

This indicates that the transition is always unstable for any $g > 0$ when the initial $K = 1/8$, and that the critical frequency is suppressed for larger initial K .

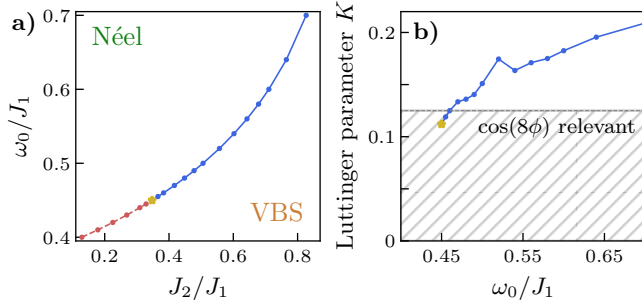


FIG. 12. Phase diagram of the spin-phonon model with $\Delta_1 = 4, \Delta_2 = 1, g = 0.15J_1$. In the limit $\omega_0 \rightarrow \infty$, the corresponding spin model undergoes a DQCP with $K_0 \approx 0.20$. The line of continuous transitions terminates at $K' \approx 1/8$, as in Fig. 1, confirming that deconfined criticality breaks down at $K' = 1/8$ independent of the initial Luttinger parameter K .

Appendix D: Additional data

In Fig. 12 we present the phase diagram for an additional phase diagram with $\Delta_1 = 4, \Delta_2 = 1, g = 0.15J_1$. For these parameters, the spin-only model H_s undergoes a DQCP with Luttinger parameter $K \approx 0.20$. Tuning ω_0/J_1 , we determine the critical frequency ω_c/J_1 from the VBS Binder cumulant as outlined in the main text. We find that the DQCP line again terminates at $K'(\omega_c) \approx 1/8$, demonstrating that the breakdown of DQC occurs at $K' = 1/8$ independent of the Luttinger parameter K of the underlying transition.

In Fig. 4 of the main text, we show that the critical order parameter exponent β and correlation length exponent ν , governing the power laws $\hat{O} \sim |J_2 - J_{2c}|^\beta$ and $\xi \sim |J_2 - J_{2c}|^{-\nu}$ are consistent with the field theory prediction $K = \beta/\nu$. In Fig. 13, we show $\beta(\omega_0)$ and $\nu(\omega_0)$ for frequencies $0.45J_1 \approx \omega_c \leq \omega_0 \leq 0.6J_1$ close to the critical endpoint of the phase diagram in Fig. 1. We determine β and ν via the mean of the longest plateau in the discrete log-log derivative, e.g. $\beta = \partial \log(\hat{O}(|J_2 - J_{2c}|)) / \partial \log(|J_2 - J_{2c}|)$. The numerical data demonstrates good agreement between the critical exponents β_M and β_Ψ of the order parameters along the whole frequency range. Moreover, the resulting ratios β/ν agree with the estimates of the Luttinger parameter K obtained in the main text.

In Sec. III B, we argue that the transition at the critical frequency ω_c lies in the 4-state Potts universality class and employ a finite-size scaling Ansatz to obtain the critical exponents β and ν . The idea behind the ansatz

$$\hat{O}\chi^{\beta\kappa/\nu} = F(\delta J_2 \chi^{\kappa/\nu}), \quad (\text{D1})$$

where $\delta J_2 \equiv (J_2 - J_{2c})/J_{2c}$ is as follows: At criticality, the exponent $\kappa = 6/(c(\sqrt{12/c}+1))$ relates the MPS bond dimension $\chi^\kappa = \xi(\chi)$ to the MPS correlation length ξ via finite entanglement scaling [48, 54]. The Ansatz can then be understood in terms of the usual finite-size scaling ansatz $\hat{O}L^{\beta/\nu} = f(\delta J_2 L^{1/\nu})$ with effective length scale $L \sim \xi_\chi \sim \chi^\kappa$.

We confirm the critical exponents β and ν in Fig. 14 for a sweep along the frequency direction, keeping $J_{2c}(\omega_c = 0.45J_1) = 0.14546J_1$ fixed and varying ω_0/J_1 . We obtain $\beta_M = 0.078, \beta_\Psi = 0.09$ and $\nu = 0.635$, in good agreement with previous estimates in Fig. 6 and the exact 4-state Potts values $\beta = 1/12, \nu = 2/3$. The result confirms that the four-Potts critical exponents are found independent of the chosen sweep direction.

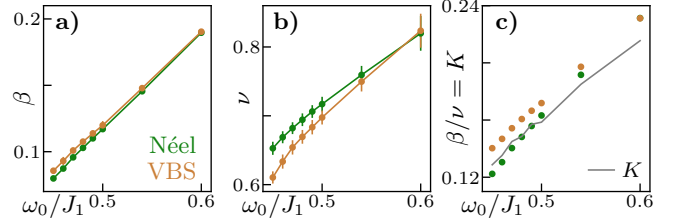


FIG. 13. a,b) Critical exponents β and ν determined via discrete log-log derivatives, for frequencies close to the critical endpoint shown in Fig. 1. c) The estimate $K = \beta/\nu$ is consistent with previous estimates of the Luttinger parameter K (gray line) obtained in the main text.

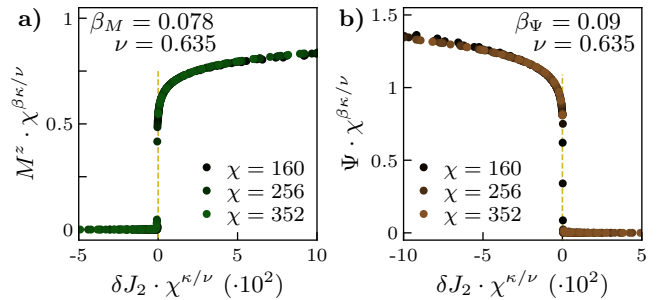


FIG. 14. Critical exponents β and ν obtained from a sweep along the frequency direction at the critical endpoint $\omega_c = 0.45J_1$ discussed in the main text. The resulting values are consistent with those obtained from the sweep in J_2 -direction shown in Fig. 6.